CRYSTAL GROWTH & DESIGN

Article

pubs.acs.org/crystal

Tetrahedral Polyoxometalate Nanoclusters with Tetrameric Rare-Earth Cores and Germanotungstate Vertexes

Junwei Zhao,*[,†,‡] Dongying Shi,[†] Lijuan Chen,*[,†] Pengtao Ma,[†] Jingping Wang,[†] Jian Zhang,*[,‡] and Jingyang Niu*[,†]

[†]Institute of Molecular and Crystal Engineering, Henan Key Laboratory of Polyoxometalate Chemistry, College of Chemistry and Chemical Engineering, Henan University, Kaifeng, Henan 475004, People's Republic of China

[‡]State Key Laboratory of Structural Chemistry, Fujian Institute of Research on the Structure of Matter, Chinese Academy of Sciences, Fuzhou, Fujian 350002, People's Republic of China

Supporting Information

ABSTRACT: Two novel 1D copper-bridged tetrahedral polyoxometalate nanoclusters with tetrameric rare-earth cores and germanotungstate vertexes, $Na_3H_7[Cu(en)_2]_5[Cu(en)_2(H_2O)]_2[RE_4Ge_4W_{46}O_{164}(H_2O)_3]\cdot nH_2O$ (RE = Gd^{III}, n = 25 for **1**; RE = Y^{III}, n = 23 for **2**; en = ethylenediamine), have been hydrothermally synthesized and structurally characterized by elemental analyses, IR spectra, thermogravimetric analysis (TGA), and single-crystal X-ray diffraction. The most prominent structural feature of **1** and **2** consists of unprecedented tetrahedral RE-substituted germanotungstate nanoclusters $\{[(\alpha\text{-}GeW_{11}O_{39}RE)_2(\mu_3\text{-}WO_4)(\alpha\text{-}GeW_{11}O_{39}RE(H_2O))](\mu_4\text{-}WO_4)[\alpha\text{-}GeW_{11}O_{39}RE(H_2O)_2]\}^{24-}$, in which four mono-$RE^{III}$-substituted Keggin $[\alpha\text{-}GeW_{11}O_{39}RE(H_2O)_n]^{5-}$ (n = 0, 1, 2) moieties are combined together with the aid of two WO_4^{2-} connectors. What's more interesting is that adjacent tetrahedral nanoclusters are interconnected with each other via $[Cu(en)_2]^{2+}$ bridges, forming a 1D extended chain architecture. To our knowledge, **1** and **2** are the first polyoxometalate-based Cu–RE containing 1D chain constructed from tetrahedral RE-substituted germanotungstate nanoclusters and copper–organic bridges. Furthermore, the solid-state electrochemical and electrocatalytic properties of **1** and **2** have been carried out in 0.5 mol·L^{-1} Na_2SO_4 + H_2SO_4 aqueous solution by entrapping them in a carbon paste electrode. **1** and **2** display apparent electrocatalytic activities for the nitrite and bromate reduction.

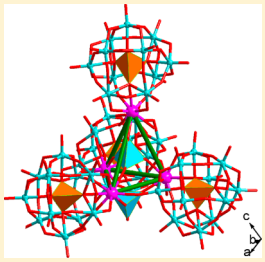

INTRODUCTION

Polyoxometalates (POMs) are a versatile family of metal–oxygen clusters with oxygen-rich surfaces and a controllable size, shape, composition, charge density, solubility, redox potential, and acid strength, which are widely studied in different scientific domains, such as catalysis, magnetism and nanotechnology, electrochemistry, photochemistry, and materials science.[1] The design and synthesis of large metal oxide clusters are in the current forefront of synthetic chemistry. The self-assembly of large clusters often proceeds via condensation steps, which is usually thermodynamically driven by charge and nucleophilicity of the growing transient cluster fragments.[2]

Lacunary POMs are inorganic multidentate ligands that can integrate multinuclear d- or f-block metals, offering the possibility of combining stereospecific elements (mainly transition-metal (TM) and rare-earth (RE) cations) in structurally diverse multiunit assemblies. Such an enormous potential has given rise to a dramatic increase in the number and size of TM-substituted POMs (TMSPs) and RE-substituted POMs (RESPs) with specific properties for applications.[3] A simple synthetic strategy is based upon the self-assembly of preformed defect POM precursors with TM or RE cations.[4,5] By this way, Yamase et al. prepared tetrameric and hexameric RESPs $[Cs\subset\{Eu(H_2O)_2(\alpha\text{-}AsW_9O_{33})\}_4]^{23-}$ and $[K\subset\{Eu(H_2O)_2(\alpha\text{-}AsW_9O_{33})\}_6]^{35-}$ in 2005.[4a] Godin et al. reported a hexameric TMSP $[H_{56}P_8W_{48}Fe_{28}O_{248}]^{28-}$.[4b] Kortz and co-workers described a 20 Ce^{III} containing decamer $[Ce_{20}Ge_{10}W_{100}O_{376}(OH)_4(H_2O)_{30}]^{56-}$.[4c] Later, Yang et al. addressed a tetrameric TMSP $[\{Fe^{II}_{1.5}Fe^{III}_{12}(\mu_3\text{-}OH)_{12}(\mu_4\text{-}PO_4)_4\}(B\text{-}\alpha\text{-}PW_9O_{34})_4]^{21-}$.[4d] Wang et al. obtained two multicopper containing tetramers $[Cu_{14}(OH)_4(H_2O)_{16}(SiW_8O_{31})_4]^{16-}$ and $[Cu_{10}(H_2O)_2(N_3)_4(GeW_9O_{34})_2(GeW_8O_{31})_2]^{24-}$.[4e] In 2009, Hussain and co-workers synthesized a Gd^{III}-bridged polytungstoarsenate nanocluster $[Gd_8As_{12}W_{124}O_{432}(H_2O)_{22}]^{60-}$.[4f] In 2010, Reinoso et al. communicated a giant crown-shaped polytungstate $[K\subset K_7Ce_{24}Ge_{12}W_{120}O_{456}(OH)_{12}(H_2O)_{64}]^{52-}$.[4g] Recently, Fang et al. discovered a gigantic core–shell TMSP $[Mn^{III}_{40}P_{32}W^{VI}_{224}O_{888}]^{144-}$.[2] Kortz's group isolated a planar $\{Mn_{19}(OH)_{12}\}^{26+}$ unit incorporated in a 60-tungsto-6-silicate polyanion $[Mn_{19}(OH)_{12}(SiW_{10}O_{37})_6]^{34-}$.[4h] Most reported large TMSP or RESP clusters are, however, discrete in structure. The extended architectures established by large TMSP or RESP clusters are rare, but some examples are reported, which include a 1D phosphotungstate made up of 20 Ni^{II} substituted $\{Ni_{20}P_4W_{34}(OH)_4O_{136}(en)_9(H_2O)_4\}$ units communicated by Yang's group,[5a] two 1D arsenotungstates built by 18 Ni^{II} substituted $\{[(\alpha\text{-}AsW_6O_{26})Ni_6(OH)_2(H_2O)_3(en)(B\text{-}\alpha\text{-}AsW_9O_{34})]_2$-

Received: May 14, 2013
Revised: July 26, 2013
Published: August 13, 2013

Table 1. X-ray Diffraction Crystallographic Data for 1 and 2

	1	2
empirical formula	$C_{28}H_{179}Cu_7Gd_4Ge_4N_{28}Na_3O_{194}W_{46}$	$C_{28}H_{175}Cu_7Ge_4N_{28}Na_3O_{192}W_{46}Y_4$
formula weight	13903.20	13593.81
crystal system	triclinic	triclinic
space group	$P\bar{1}$	$P\bar{1}$
a, Å	21.635(2)	21.675(2)
b, Å	23.415(3)	23.348(2)
c, Å	24.754(3)	24.687(2)
α, deg	93.327(2)	93.355(2)
β, deg	100.308(2)	100.387(2)
γ, deg	97.322(2)	97.351(2)
V, Å^3	12 195(2)	12 145(2)
Z	2	2
absorption coefficient, mm^{-1}	23.849	23.815
F(000)	12 238	11 998
T, K	296(2)	296(2)
limiting indices	$-25 \le h \le 25$	$-25 \le h \le 25$
	$-27 \le k \le 27$	$-27 \le k \le 27$
	$-24 \le l \le 29$	$-29 \le l \le 20$
no. of reflns collected	62 356	61 678
no. of independent reflns	42 577	42 392
R_{int}	0.0770	0.0918
data/restrains/parameters	42577/657/2291	42392/521/2474
goodness-of-fit on F^2	1.008	1.006
final R indices [$I > 2\sigma(I)$]	$^aR_1$ = 0.0792	R_1 = 0.0788
	$^bwR_2$ = 0.1368	wR_2 = 0.1306
R indices (all data)	R_1 = 0.1558	R_1 = 0.1602
	wR_2 = 0.1493	wR_2 = 0.1397

$^aR_1 = \sum||F_o| - |F_c||/\sum|F_o|$. $^bwR_2 = [\sum w(F_o^2 - F_c^2)^2/\sum w(F_o^2)^2]^{1/2}$; $w = 1/[\sigma^2(F_o^2) + (xP)^2 + yP]$, $P = (F_o^2 + 2F_c^2)/3$, where $x = 0.0222$, $y = 0.0000$ for **1**, $x = 0.0278$, $y = 0.0000$ for **2**.

$[W_4O_{16}][Ni_3(H_2O)_2(en)]_2\}^{16-}$ and 20 Ni^{II} substituted $\{[(\alpha\text{-}AsW_6O_{26})Ni_6(OH)_2(en)_{2.5}(B\text{-}\alpha\text{-}AsW_9O_{34})]_2H_4[W_4O_{16}][Ni_4(H_2O)_2(en)_2]_2\}^{8-}$ units addressed by us,[5b] and an accessible open framework nanocube-based architecture $[Mn_8(H_2O)_{48}P_8W_{48}O_{184}]^{24-}$ discovered by Cronin et al.[5c]

Hitherto, extended architectures created by large TM-bridged large RESPs or RE-bridged large TMSPs have been less explored. The challenge lies in the unavoidable competition among highly negative POM precursors, less-active TM cations, and strongly oxyphilic RE cations in the reaction system.[6] In this work, by reactions of the lacunary germanotungstate (GT) precursor with Cu^{II} and RE^{III} cations under hydrothermal conditions, we first realize unusual 1D copper-bridged tetrahedral POM nanoclusters with a tetrameric RE core and GT vertexes. Two rare 1D copper-bridged RESP architectures, $Na_3H_7[Cu(en)_2]_5[Cu(en)_2(H_2O)]_2[RE_4Ge_4W_{46}O_{164}(H_2O)_3]\cdot nH_2O$ (RE = Gd^{III}, n = 25 for **1**; RE = Y^{III}, n = 23 for **2**; en = ethylenediamine), have been successfully synthesized and structurally characterized. To our knowledge, both represent the first 1D POM-based structures constructed from tetrameric RE-substituted GT nanoclusters and copper−organic linkers. This finding provides a route for preparing the extended structures made by large TM−RE containing POM units. Such a tetrahedral nanocluster represents the third largest GT cluster characterized so far, being only surpassed by $[Ce_{20}Ge_{10}W_{100}O_{376}(OH)_4(H_2O)_{30}]^{56-}$,[4c] and $[K\subset K_7Ce_{24}Ge_{12}W_{120}O_{456}(OH)_{12}(H_2O)_{64}]^{52-}$.[4g] TGA measurements of **1** and **2** have been performed and are used to determine the lattice water molecules of **1** and **2**. The cyclic voltammograms from **1** or **2** modified carbon paste electrodes exhibit two pairs of redox waves, which are, respectively, attributable to the redox process of the Cu^{II} centers and the redox process of the W^{VI} centers in the framework. Moreover, the W^{VI}-based waves of **1** or **2** modified carbon paste electrodes manifest obvious electrocatalytic activities for the nitrite and bromate reduction.

EXPERIMENTAL SECTION

Materials and Methods. The trivacant Keggin GT precursor $K_8Na_2[A\text{-}\alpha\text{-}GeW_9O_{34}]\cdot 25H_2O$[7] was synthesized as previously described. All other chemicals were used as purchased without purification. Elemental analyses (C, H, and N) were performed using a PerkinElmer 240C elemental analyzer. IR spectra were obtained from a sample powder palletized with KBr on a Nicolet 170 SXFT−IR spectrophotometer over the range of 4000−400 cm^{-1}. TGA experiments were performed under a N_2 atmosphere on a Mettler-Toledo TGA/SDTA851 instrument with the heating rate of 10 °C min^{-1} from 25 to 800 °C. Cyclic voltammograms were recorded on a CS electrochemical workstation (Wuhan Corrtest Instrument Co. LTD) at room temperature. A conventional three-electrode system was used. Platinum gauze was used as a counter electrode, and a Ag/AgCl electrode was referenced. Chemically bulk-modified carbon paste electrodes (CPEs) were used as working electrodes. A PHB-4 type pH meter was used for pH measurement.

Synthesis of $Na_3H_7[Cu(en)_2]_5[Cu(en)_2(H_2O)]_2[Gd_4Ge_4W_{46}O_{164}(H_2O)_3]\cdot 25H_2O$ (1). A mixture of $K_8Na_2[A\text{-}\alpha\text{-}GeW_9O_{34}]\cdot 25H_2O$ (0.330 g, 0.107 mmol), $CuCl_2\cdot 2H_2O$ (0.068 g, 0.399 mmol), $GdCl_3$ (0.068 g, 0.258 mmol), en (0.10 mL, 1.494 mmol), and H_2O (5 mL, 278 mmol) was stirred for 2 h, sealed in a 25 mL Teflon-lined steel autoclave, kept at 160 °C for 6 days, and then cooled to room temperature. Purple prismatic crystals of **1** were obtained by filtering, washed with distilled water, and then dried at ambient temperature. Yield: ca. 32% (based on $K_8Na_2[A\text{-}\alpha\text{-}GeW_9O_{34}]\cdot 25H_2O$). Elemental

dx.doi.org/10.1021/cg400746n | Cryst. Growth Des. 2013, 13, 4368−4377

analysis for $C_{28}H_{179}Cu_7Gd_4Ge_4Na_3N_{28}O_{194}W_{46}$: C, 2.42; H, 1.30; N, 2.82. Found: C, 2.58; H, 1.47; N, 2.74.

Synthesis of $Na_3H_7[Cu(en)_2]_5[Cu(en)_2(H_2O)]_2[Y_4Ge_4W_{46}O_{164}(H_2O)_3]\cdot 23H_2O$ (2). The synthetic procedure of **1** was employed with a mixture of $K_8Na_2[A\text{-}\alpha\text{-}GeW_9O_{34}]\cdot 25H_2O$ (0.431 g, 0.140 mmol), $CuCl_2\cdot 2H_2O$ (0.063 g, 0.370 mmol), YCl_3 (0.068 g, 0.348 mmol), en (0.10 mL, 1.494 mmol), and H_2O (5 mL, 278 mmol). The reaction time was changed to 9 days; purple prismatic crystals were obtained. Yield: ca. 35%. Elemental analysis for $C_{28}H_{175}Cu_7Ge_4N_{28}Na_3O_{192}W_{46}Y_4$: C, 2.47; H, 1.30; N, 2.89. Found: C, 2.60; H, 1.45; N, 2.85.

Preparations of 1- and 2-CPEs. **1**-CPE was fabricated as follows: 30 mg of graphite powder and 10 mg of **1** were mixed and ground together by an agate mortar and pestle to achieve a uniform mixture, and then 0.05 mL of nujol was added with stirring. The homogenized mixture was packed into a glass tube with a 3.0 mm inner diameter, and the tube surface was wiped with paper. Electrical contact was established with a Cu rod through the back of the electrode. In a similar manner, **2**-CPE was made with compound **2**.

Gas Adsorption Measurements. Low-pressure gas adsorption measurements involved in this work were performed at 77 K for N_2 and H_2, maintained by a liquid nitrogen bath, on a Quantachrome Quadrasorb automatic volumetric instrument. CO_2 adsorption measurements were done at 198 K. In all adsorption measurements, ultra-high-purity H_2 was obtained by using calcium aluminosilicate adsorbents to remove trace amounts of water and other impurities before introduction into the system. The crystals of **1** and **2** were heated at 130 °C for 6 h under a dynamic vacuum to remove water molecules.

X-ray Crystallography. The intensity data collections for **1** and **2** were carried out at 296 K using a Bruker Apex II diffractometer equipped with a CCD bidimensional detector with the graphite-monochromated Mo Kα radiation (λ = 0.71073 Å). The absorption correction was based on multiple and symmetry-equivalent reflections in the data set using the SADABS program.[8a] Direct methods were used to solve the structures and to locate the heavy atoms using the SHELXTL-97 program package.[8b,c] The remaining atoms were found from successive full-matrix least-squares refinements on F^2 and Fourier syntheses. No hydrogen atoms associated with water molecules were located from the difference Fourier map. Hydrogen atoms attached to carbon and nitrogen atoms were geometrically placed. All hydrogen atoms were refined isotropically as a riding mode using the default SHELXTL parameters. All non-hydrogen atoms were refined anisotropically except for some oxygen, carbon, and nitrogen atoms and water molecules (see the Supporting Information). Crystallographic data and structure refinements for **1** and **2** are summarized in Table 1.

RESULTS AND DISCUSSION

Synthesis. In the past several decades, intensive interest has been devoted to the search and discovery of TM-, RE-, or organometal (OM)-substituted POMs.[4,5,9] One of the important synthetic strategies is incorporation of TM, RE, or OM cations into the defect sites of POM lattices to construct a tremendous number of POM-based materials with various stoichiometries and structural features combined with interesting properties. Within the class of POM candidates, lacunary polyoxotungstates are particularly important in this respect on account of their higher stability than polymolybdates and polyvanadates.[9l] Lacunary Keggin GT precursors as the crucial members of them have been also exploited (Table S1, Supporting Information).[10,11] As shown in Table S1, so far, most of the previously reported work has been primarily focused on the preparations and characterization of congeneric metal-substituted GTs; however, the combination of lacunary GT precursors with heterogeneous metal ions to synthesize newfangled TM−RE containing GTs remains less explored.[w,y,11c] On one hand, lately, the search and discovery of POM-based TM−RE containing species have gradually become a new growth point of POM chemistry. On the other hand, the current trend of synthetic chemistry is toward "rational design" based on the accumulated knowledge of crystal chemistry, thermodynamics, and reactivity principles as well as the relationship between structures and properties.[9d] Enlightened by this context, with the aim of discovering novel organic−inorganic hybrid TM-bridged RESPs or RE-bridged TMSPs, the system containing the $[A\text{-}\alpha\text{-}GeW_9O_{34}]^{10-}$ precursor and Cu^{2+} and RE^{3+} cations has been continuously and extensively exploited based on the following considerations: (a) The trivacant $[A\text{-}\alpha\text{-}GeW_9O_{34}]^{10-}$ precursor is the readily accessible and the most used GT candidate and has the relatively high activity in the aqueous solution. (b) Compared with other TM cations, Cu^{II} ions exhibit more flexible various coordination modes (square, trigonal bipyramid, square pyramid, and octahedron); moreover, the Jahn−Teller effect of the octahedron and pseudo-Jahn−Teller effect of the square pyramid for Cu^{II} cations can make them adopt diverse linking modes to overcome steric hindrance, forming novel architectures.[9m] (c) RE cations provide good opportunities for discovering unusual structures due to their high and variable coordination numbers and flexible coordination geometry. (d) The combination of flexible coordinate Cu^{II} and RE^{III} ions with lacunary GT precursors tends to construct unique TM-bridged RESPs or RE-bridged TMSPs.

First of all, when the reaction was performed with $K_8Na_2[A\text{-}\alpha\text{-}GeW_9O_{34}]\cdot 25H_2O/CuCl_2\cdot 2H_2O/LaCl_3$ in the presence of en, a novel tetrameric TM−RE containing GT $Na_2H_6[Cu(en)_2(H_2O)]_8\{Cu(en)_2[La(\alpha\text{-}GeW_{11}O_{39})_2]_2\}\cdot 18H_2O$ was first discovered, and its major skeleton $\{Cu(en)_2[La(\alpha\text{-}GeW_{11}O_{39})_2]_2\}^{24-}$ is made up of two 1:2-type $[La(\alpha\text{-}GeW_{11}O_{39})_2]^{13-}$ moieties and one $[Cu(en)_2]^{2+}$ linkage.[11c] To investigate the influence of other RE ions on the structures of Cu−RE containing GTs, various reactions were performed using different RE cations. When $LaCl_3$ was replaced by $PrCl_3$ or $ErCl_3$, similar tetramers, $K_4H_2[Cu(en)_2(H_2O)_2]_5[Cu(en)_2(H_2O)]_2[Cu(en)_2]_2\{Cu(en)_2[Pr(\alpha\text{-}GeW_{11}O_{39})_2]_2\}\cdot 16H_2O$ and $KNa_2H_7[enH_2]_3Cu(en)_2(H_2O)]_2[Cu(en)_2]_2\{Cu(en)_2[Er(\alpha\text{-}GeW_{11}O_{39})_2]_2\}\cdot 15H_2O$, were also obtained.[11c] When $EuCl_3$, $TbCl_3$, and $DyCl_3$ were, respectively, utilized, three fresh members, $\{[Cu(en)_2(H_2O)][Cu_3RE(en)_3(OH)_3(H_2O)_2](\alpha\text{-}GeW_{11}O_{39})\}_2\cdot nH_2O$ (RE = Eu^{III}, Tb^{III}, n = 11, RE = Dy^{III}, n = 10), were sequentially afforded, which display the interesting dimeric motif $\{[Cu_3RE(en)_3(OH)_3(H_2O)_2](\alpha\text{-}GeW_{11}O_{39})\}_2^{4-}$ constructed from two $\{Cu_3REO_4\}$ cubane anchored monovacant $[\alpha\text{-}GeW_{11}O_{39}]^{8-}$ fragments by virtue of two W−O−RE−O−W linkers.[11c] As our work continued, the employment of $GdCl_3$ or YCl_3 resulted in the formation of two novel copper-bridged tetrahedral POM nanoclusters with 1D architectures, $Na_3H_7[Cu(en)_2]_5[Cu(en)_2(H_2O)]_2[RE_4Ge_4W_{46}O_{164}(H_2O)_3]\cdot nH_2O$ (RE = Gd^{III}, n = 25 for **1**; RE = Y^{III}, n = 23 for **2**). These results illustrate that the nature of RE^{III} cations has an important influence on the structural diversity of the resulting GT derivatives. Additionally, the common structural features of these heterometal containing GTs are that they all consist of $[\alpha\text{-}GeW_{11}O_{39}]^{8-}$ fragments; however, when $K_6Na_2[\alpha\text{-}GeW_{11}O_{39}]\cdot 13H_2O$ replaced $K_8Na_2[A\text{-}\alpha\text{-}GeW_9O_{34}]\cdot 25H_2O$ under the similar conditions, they cannot be obtained, which suggests that it seems to be indispensable for the conversion of $[A\text{-}\alpha\text{-}GeW_9O_{34}]^{10-}$ to $[\alpha\text{-}GeW_{11}O_{39}]^{8-}$ in their preparations. Extra tungsten centers are inserted into the skeletons of **1** and **2** as a result of partial decomposition or

evolution of some of the lacunary $[A\text{-}\alpha\text{-}GeW_9O_{34}]^{10-}$ precursor in solution. Alternatively, addition of extra sodium tungstate during the reaction cannot form **1** and **2**.

In the combination procedure of the $[A\text{-}\alpha\text{-}GeW_9O_{34}]^{10-}$ precursor with Cu^{2+} and RE^{3+} cations in the participation of en, some points are worthy of mentioning here: (1) hydrothermal synthesis, which is preferentially employed in favor of generating more complicated metastable or intermediate phases, offers an excellent opportunity for the formation of unique GT-based Cu−RE units. (2) The simultaneous introduction of Cu^{II} and RE^{III} cations to the bifunctional active GT (as H^+/e^- reservoirs) system in the presence of organic components not only can alter the reaction behavior of the system but also can transfer their functionalities (such as magnetic and optical properties, Lewis acid catalysis) to the targeted species with enhanced properties owing to their synergistic effects.[4g] (3) The delicate combination of Cu^{II} and RE^{III} cations with lacunary GT precursors will create unprecedented phases constituted by in situ formed huge GT-based Cu−RE units due to the flexibility of coordination modes of Cu^{II} ions and the oxophilicity and high coordination numbers of RE ions. (4) The nature of RE ions decides their activity to react with lacunary GT precursors; that is, the copper-bridged tetrahedral POM nanoclusters are only formed by the reaction of Gd^{3+} or Y^{3+} ions with $[A\text{-}\alpha\text{-}GeW_9O_{34}]^{10-}$ and Cu^{2+} ions. In addition, to investigate the effect of the nature of other TM cations on the structural diversity of the products, Ni^{2+} and Co^{2+} cations were used in the presence of RE ions under the similar conditions; unfortunately, only organic−inorganic hybrid TM sandwiched GTs, $[enH_2]_2[Ni(en)_2]_2\{[Ni_6(en)_2(H_2O)_2][B\text{-}\alpha\text{-}GeW_9O_{34}]_2\}\cdot 14H_2O$[11b] and $\{[Co(dap)_2(H_2O)]_2[Co(dap)_2]_2[Co_4(Hdap)_2(B\text{-}\alpha\text{-}HGeW_9O_{34})_2]\}\cdot 7H_2O$,[11d] were obtained. When other TM ions, such as Ti^{4+}, Cr^{3+}, Fe^{3+}, Fe^{2+}, and Cd^{2+} ions, were also investigated, however, amorphous powders were obtained. In a word, the aforementioned facts indicate that the Cu^{2+} ions have the high tendency to form the TM−RE containing GTs, whereas the Ni^{2+} or Co^{2+} ions have the strong tendency to generate the TM-substituted sandwich-type GTs in our studied system.

IR Spectra. The IR spectra of **1** and **2** have been recorded between 4000 and 400 cm^{-1} (Figure S1, Supporting Information) and display four characteristic vibration patterns derived from the Keggin framework in the low-wavenumber region. Four characteristic vibration bands attributable to $\nu(W-O_t)$, $\nu(Ge-O_a)$, $\nu(W-O_b)$, and $\nu(W-O_c)$ are observed at 943, 873, 801, and 690 cm^{-1} for **1** and 944, 874, 801, and 691 cm^{-1} for **2**, respectively. The IR spectra of **1** and **2** in the low-wavenumber region resemble that of $K_6Na_2[\alpha\text{-}GeW_{11}O_{39}]\cdot 13H_2O$ (Figure S1), indicating that they contain the monovacant Keggin $[\alpha\text{-}GeW_{11}O_{39}]^{8-}$ fragments in their skeletons. Compared to $K_6Na_2[(\alpha\text{-}GeW_{11}O_{39})]\cdot 13H_2O$, the $\nu(W-O_t)$ vibration bands for **1** and **2** are almost not shifted, suggesting that $[Cu(en)_2]^{2+}$ and $[Cu(en)_2(H_2O)]^{2+}$ cations have a weak effect on the terminal oxygen atoms on $[\alpha\text{-}GeW_{11}O_{39}]^{8-}$ fragments. The $\nu(W-O_b)$ vibration bands for **1** and **2** split into two peaks, the possible major reason for which may be related to the fact that the incorporation of the RE^{III} cations to the defect sites of the $[\alpha\text{-}GeW_{11}O_{39}]^{8-}$ fragments leads to the deformation and distortion of the $[\alpha\text{-}GeW_{11}O_{39}]^{8-}$ skeletons. The IR spectra of **1** and **2** are obviously different from that of $K_8Na_2[A\text{-}\alpha\text{-}GeW_9O_{34}]\cdot 25H_2O$ (Figure S1), which further confirms the structural transformation of the $[A\text{-}\alpha\text{-}GeW_9O_{34}]^{10-}$ precursor to the $[\alpha\text{-}GeW_{11}O_{39}]^{8-}$ fragment. For **1** and **2**, the stretching bands of $-NH_2$ and $-CH_2$ groups are observed at 3135−3309 and 2880−2945 cm^{-1} and the bending vibration bands of $-NH_2$ and $-CH_2$ groups also appear at 1579−1585 and 1452−1460 cm^{-1}. These resonance signals verify the presence of en groups in **1** and **2**.

Structural Description. X-ray analyses reveal that **1** and **2** are essentially isomorphic and consist of a large TM−RE−POM fragment containing a novel tetrahedral RE-substituted $[RE_4Ge_4W_{46}O_{164}(H_2O)_3]^{24-}$ subunit with five $[Cu(en)_2]^{2+}$ and two $[Cu(en)_2(H_2O)]^{2+}$ cations (Figures S2 and S3, Supporting Information). Thus, only the structure of **1** is briefly described here. The prominent structural feature of **1** is the presence of an unprecedented tetrahedral Gd^{III}-substituted GT subunit $\{[(\alpha\text{-}GeW_{11}O_{39}Gd)_2(\mu_3\text{-}WO_4)(\alpha\text{-}GeW_{11}O_{39}Gd(H_2O))](\mu_4\text{-}WO_4)[\alpha\text{-}GeW_{11}O_{39}Gd(H_2O)_2]\}^{24-}$ with a size of ca. 2.1 nm (Figure 1). In this special tetrahedral unit, four Keggin-type $[\alpha\text{-}GeW_{11}O_{39}Gd(H_2O)_n]^{5-}$ (n = 0, 1, 2) moieties are fused together with the help of two WO_4^{2-} ions (Figure 2). There are four crystallographically unique Gd^{III} ions (Gd1, Gd2, Gd3, and Gd4), which are all incorporated to the monovacant sites of the $[\alpha\text{-}GeW_{11}O_{39}]^{8-}$fragments through four Gd−O bonds [Gd−O: 2.25(2)−2.457(17) Å]. Notably, four Gd^{III} ions display two types of coordination geometries. The Gd1, Gd3, and Gd4 ions inhibit in the seven-coordinate severely distorted monocapped trigonal prism, whereas the Gd2 ion adopts the eight-coordinate distorted square antiprismatic configuration (Figure 3). The difference of coordination geometries of Gd^{III} ions is related to the effect of the steric hindrance. More concretely, three mono-Gd^{III}-substituted Keggin $[\alpha\text{-}GeW_{11}O_{39}Gd(H_2O)_n]^{5-}$ moieties are combined together by three W−O−Gd−O−W connectors; meanwhile, two WO_4^{2-} ions cap on

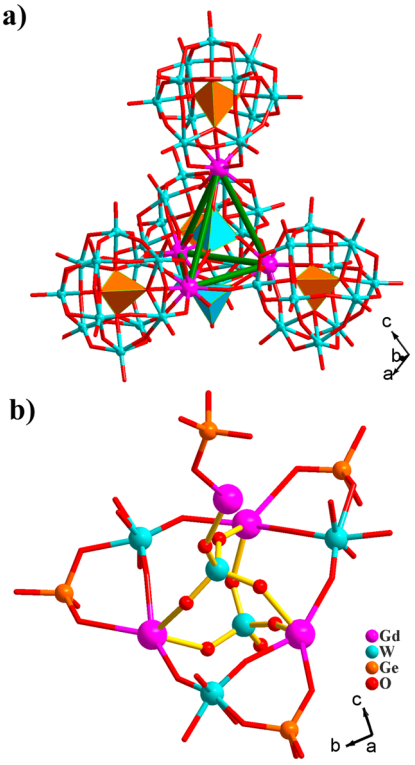

Figure 1. (a) The tetrahedral POM nanocluster with the tetrameric Gd^{III} core and GT vertexes. (b) The detailed coordination connectivity around the tetrameric Gd^{III} core.

dx.doi.org/10.1021/cg400746n | Cryst. Growth Des. 2013, 13, 4368−4377

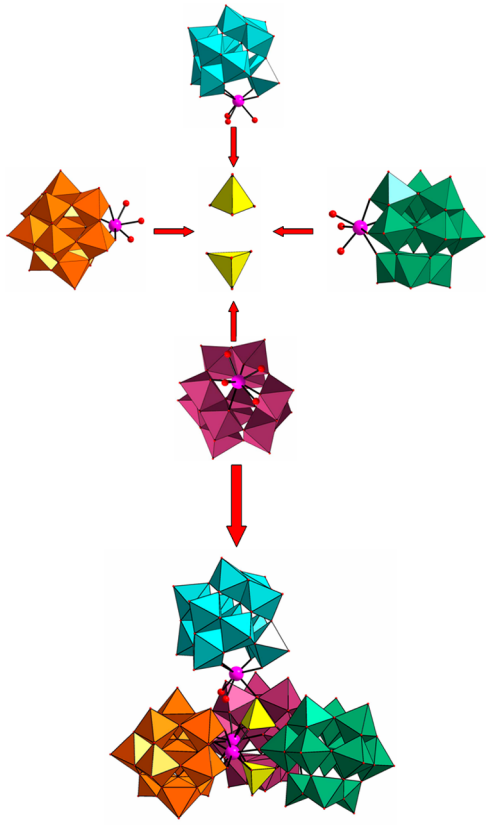

Figure 2. Top: the exploded view of $\{[(\alpha\text{-}GeW_{11}O_{39}Gd)_2(\mu_3\text{-}WO_4)(\alpha\text{-}GeW_{11}O_{39}Gd(H_2O))](\mu_4\text{-}WO_4)[\alpha\text{-}GeW_{11}O_{39}Gd(H_2O)_2]\}^{24-}$. Bottom: the arrangement of four Keggin-type $[\alpha\text{-}GeW_{11}O_{39}Gd(H_2O)_n]^{5-}$ (n = 0, 1, 2) moieties with the help of two WO_4^{2-} ions (shown in different colors for clarity).

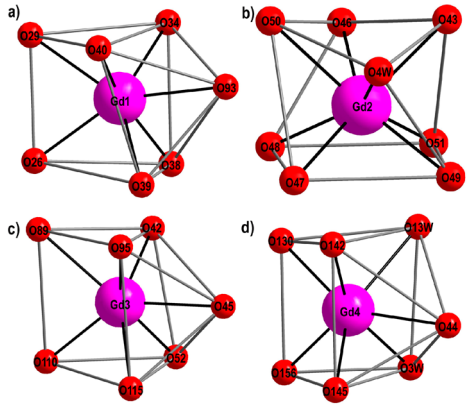

Figure 3. Coordination geometries of Gd1, Gd2, Gd3, and Gd4 ions in **1**.

both sides of the trimeric unit via coordinating to three Gd^{III} ions, generating a unique windmill-like arrangement (Figure 4a), which is completely distinct from the other reported trimers, such as $[Co(H_2O)_3(\alpha\text{-}GeW_{11}CoO_{38})_3]^{10-}$,[11a] $[(\beta_2\text{-}SiW_{11}MnO_{38}OH)_3]^{15-}$,[12] and $[Rb\subset(GeW_{10}Mn_2O_{38})_3]^{17-}$.[10o] More interestingly, to reduce the steric hindrance, the fourth Keggin $[\alpha\text{-}GeW_{11}O_{39}Gd(H_2O)_2]^{5-}$ moiety grafts to the $\mu_4\text{-}WO_4^{2-}$ ion via only one Gd−O−W bond, thus constructing the novel tetrahedral poly(POM) nanocluster. As a result, this nanocluster can be approximately viewed as the product of a $\mu_4\text{-}WO_4^{2-}$-directed tetrahedral assembly of four Keggin $[\alpha\text{-}GeW_{11}O_{39}Gd(H_2O)_n]^{5-}$ subunits. Actually, the presence of the $\mu_3\text{-}WO_4^{2-}$ ion to some extent prevents the distribution of four $[\alpha\text{-}GeW_{11}O_{39}Gd(H_2O)_n]^{5-}$ moieties in the form of a regular tetrahedron. As a result, the $\mu_4\text{-}WO_4^{2-}$ ion is not situated on the center of the tetrahedron, which is further confirmed by the distorted tetrahedral alignments of four Gd^{III} ions and four $[\alpha\text{-}GeW_{11}O_{39}]^{8-}$ fragments (Figure 4b, Figure S4, Supporting Information). It should be noted that the construction mode of such a nanocluster is first observed and distinct from those of the reported tetrameric TMSP or RESP clusters, such as $[Nb_4O_6(\alpha\text{-}Nb_3SiW_9O_{40})_4]^{20-}$,[9j] $[(PM_2W_{10}O_{38})_4(W_3O_{14})]^{30-}$ (M = Eu^{III}, Y^{III}),[9a] $[\{(SiW_9O_{34})(SiW_9O_{33}(OH))(Cu(OH))_6Cu\}_2X]^{23-}$ (X = Cl, Br),[9k] and $[\{Co_4(OH)_3PO_4\}_4(PW_9O_{34})_4]^{28-}$.[13] In addition, on the basis of the charge balance consideration, seven protons should be added to the molecular structural unit of **1**. Seven protons in **1** can be localized, and monoprotonated oxygen atoms are identified by bond valence sum (BVS) calculations (Table S2, Supporting Information).[14] The results show that the BVS values (1.57, 1.30, 1.57, 1.16, 1.04, 1.53, and 1.57) of O28, O39, O71, O78, O102, O105, and O139 are significantly lower than 2, indicating that two oxygen atoms may be monoprotonated. Therefore, the molecular structural unit of **1** can also be formulated as $Na_3[Cu(en)_2]_5[Cu(en)_2(H_2O)]_2[Gd_4Ge_4W_{46}H_7O_{164}(H_2O)_3]\cdot 25H_2O$. A combination of elemental analysis and TGA confirms the number of lattice water molecules in **1**. TGA indicates the presence of 25 lattice water molecules in **1** (Figure S5, Supporting Information). Similarly, there are 23 lattice water molecules in **2**. This method that determines the number of lattice water molecules for a compound is often used in giant poly(POM) species.[15]

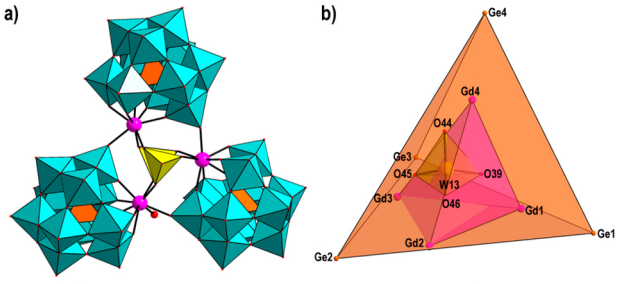

Figure 4. (a) The unique windmill-like arrangement derived from the combination of three mono-Gd^{III}-substituted Keggin $[\alpha\text{-}GeW_{11}O_{39}Gd(H_2O)_n]^{5-}$ moieties with the help of two WO_4^{2-} ions. (b) Three groups of tetrahedra in $\{[(\alpha\text{-}GeW_{11}O_{39}Gd)_2(\mu_3\text{-}WO_4)(\alpha\text{-}GeW_{11}O_{39}Gd(H_2O))](\mu_4\text{-}WO_4)[\alpha\text{-}GeW_{11}O_{39}Gd(H_2O)_2]\}^{24-}$.

More importantly, the ample oxygen surface of this nanocluster provides an excellent opportunity for the coordination of the copper−en cations in its periphery, which offers a precondition of the extended structures. In fact, the $[Cu(en)_2]^{2+}$ and $[Cu(en)_2(H_2O)]^{2+}$ ions are all bonded to this nanocluster through weak Cu−O interactions. It is interesting that adjacent tetrahedral nanoclusters are interconnected with each other via $[Cu(en)_2]^{2+}$ linkers, giving rise to a 1D chain along the c axis (Figure 5a). To the best of our knowledge, this is the first POM-based Cu−RE heterometallic 1D chain constructed from tetrahedral RE-substituted GT nanoclusters and copper−organic bridges. Furthermore, these nanocluster-based 1D chains are packing into a 3D framework with a much dense structure, which is further stabilized via extensive H-bonds between en ligands and surface oxygen atoms from adjacent **1a** subunits/water molecules (Figure 5b; Figures S6

dx.doi.org/10.1021/cg400746n | Cryst. Growth Des. 2013, 13, 4368−4377

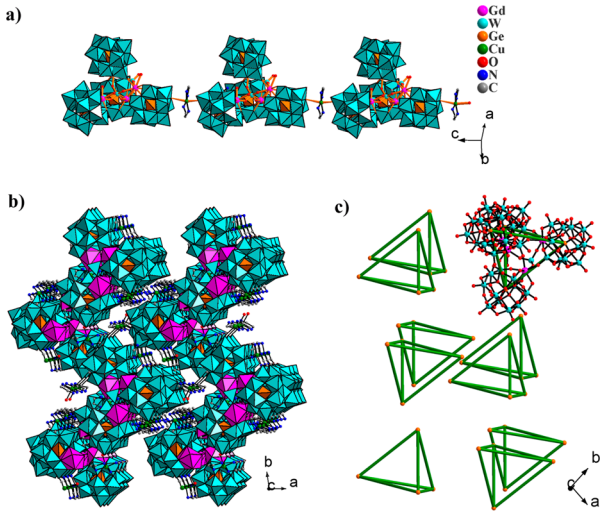

Figure 5. (a) The 1D chain formed from $[Cu(en)_2]^{2+}$-bridged tetrahedral nanoclusters. (b) The 3D structure of **1**. (c) Representation of the packing of tetrahedral nanoclusters.

and S7, Table S3, Supporting Information). The 3D packing of 1D chains forms the oblong channels with sizes of ca. 18.0 × 3.0 Å (Figure S6, Supporting Information), which are occupied by Na^+ ions and lattice water molecules, and these Na^+ ions and lattice water molecules can further stabilize the crystal structure. Actually, in the solid state, the 1D chains align side by side, thus delimiting no void in its structure, which has been also proved by the fact that **1** does not display the obvious gas-adsorption properties (Figures S8–S10, Supporting Information). In addition, the 3D structure can also be looked upon as the rational assembly of tetrahedral nanoclusters (Figure 5c).

Thermal Properties. To examine the thermal stability and determine the number of lattice water molecules of **1** and **2**, the TGA measurements of **1** and **2** have been performed on the crystalline samples under a N_2 atmosphere with a heating rate of 10 °C/min in the temperature range of 25–800 °C (Figure S5, Supporting Information). The TGA curve indicates that **1** loses weight in two steps. The weight loss of 3.64% in the first step from 25 to 225 °C corresponds to the loss of 25 lattice water molecules (calcd 3.24%). Above 140 °C, the second weight loss of 7.61% up to 800 °C is assigned to the removal of 5 coordination water molecules and 14 en ligands and the dehydration of 7 protons (calcd 7.15%). The TGA curve of **2** also shows two steps of weight loss. The first weight loss of 3.46% between 25 and 242 °C corresponds to the loss of 23 lattice water molecules (calcd 3.05%). The second weight loss of 8.20% from 242 to 800 °C is attributable to the removal of 5 coordination water molecules and 14 en ligands and the dehydration of 7 protons (calcd 7.31%). The observed experimental values are in good agreement with the elemental analyses and the results of single-crystal X-ray structural analyses.

Electrochemical and Electrocatalytic Properties. Electrochemistry of POMs has been attracting extensive interest due to their potential applications in electrocatalytic processes and the manufacture of chemically modified electrodes.[16] Extensive studies have shown that POMs are capable of delivering the electrons to other species, thus serving as the powerful electron reservoirs for multielectron reductions and electrocatalytic processes.[17] As a result, by means of cyclic voltammetry (CV), the solid-state electrochemical and electrocatalytic properties of **1** and **2** have been carried out in 0.5 mol·L^{-1} Na_2SO_4 + H_2SO_4 aqueous solution (a medium suitable for testing electrocatalytic processes) by entrapping them in a carbon paste electrode (CPE) for the sake of the inorganic–organic hybrids **1** and **2** prepared by the hydrothermal reaction being insoluble in water and having poor solubility in common organic solvents. The reproducibility of cyclic voltammograms indicates that **1**-CPE and **2**-CPE are stable in this medium. Furthermore, because **1** and **2** are isostructural, the results of CV measurements also prove that their electrochemical and electrocatalytic properties are very similar (Figures 6 and 7; Figures S11–S13, Supporting Information); as a result, only **1** is herein discussed. Figure 6a shows the typical CV behavior of **1** in a pH 1.51 sulfate medium (0.5 mol·L^{-1} Na_2SO_4 + H_2SO_4) at a scan rate of 50 mV s^{-1} at room temperature. It can be clearly seen that, in the potential range of 0.4 to −0.8 V, the patterns are restricted to two pairs of redox waves and their mean peak potentials $E_{1/2} = (E_{pa} + E_{pc})/2$ are −0.016 and −0.609 V (vs the Ag/AgCl electrode), respectively. As expected, the W^{VI}-based wave is located at a more negative potential than that attributed to the Cu^{II} centers. The former features the redox process of the Cu^{II} centers,[18] and the latter is attributed to the redox process of the W^{VI} centers in the polyoxoanion framework.[4e,7] The domain where the W^{VI} wave appears has been also observed in the other tungsten containing POMs.[19] The peak potential separation of the W^{VI}-based wave is around 120 mV, which corresponds to a semireversible one-electron charge-transfer process. Furthermore, the influence of the scan rate on electrochemical behavior of **1**-CPE has been studied in the potential range of 0.4 to −0.8 V in the above-mentioned conditions. Figure 6b illustrates the variation of cathodic peak currents of the W^{VI}-based wave with the scan rate. When the scan rate is varied from 20 to 100 mV s^{-1}, the peak current intensities (I_{pc}) are proportional to the scan rate (ν), and its linear equation is $I_{pc} = -0.000093\nu - 0.6467$ with the correlation coefficient of 0.9932, which suggests a surface-controlled electron-transfer process occurring at **1**-CPE.[16b,20] It is well-known that reduction of POMs leads to an accumulation of negative charge, which increases the basicity of the POM polyoxoanion.[20,21] Thus, the reduction process may be accompanied by concomitant protonation. To investigate the influence of the variation of the acidity on the electrochemical response of **1**-CPE (Figure 6c), H_2SO_4 was used to adjust the pH values of the 0.5 mol·L^{-1} Na_2SO_4 medium. The results indicate that the pH of the supporting electrolyte has a marked effect on the electrochemical behavior of **1**-CPE. It can be seen that, along with increasing the pH, the peak potential of the W^{VI}-based wave gradually shifts to the negative potential direction and the peak currents gradually decrease. It can be explained by the fact that reduction of **1**-CPE is accompanied by the evolution of protons from solution to the surface of the electrode to maintain charge neutrality.[17b] Along with increasing pH, slower penetration of protons to the surface of **1**-CPE should be the reason for the current decrease,[17b,22a] and the negative shift of the reduction peak potential can be elucidated by the Nernst equation.[17b,22b] This phenomenon has been observed in the Dawson-type heteropolyoxomolybdate-modified electrodes (such as $[BMIM]_6P_2Mo_{18}O_{62}$ immobilized on a glass carbon electrode, $K_6P_2Mo_{18}O_{62}\cdot 14H_2O$ assembled CNTP electrode).[20,23] In addition, Keita et al. performed the comparison studies on the solution electrochemistry and solid-state electrochemistry of $Cs_{14}Na_{22}[\{Sn(CH_3)_2(H_2O)\}_{24}\{Sn(CH_3)_2\}_{12}(A\text{-}PW_9O_{34})_{12}]\cdot 149H_2O$, and the results also indicate

dx.doi.org/10.1021/cg400746n | Cryst. Growth Des. 2013, 13, 4368–4377

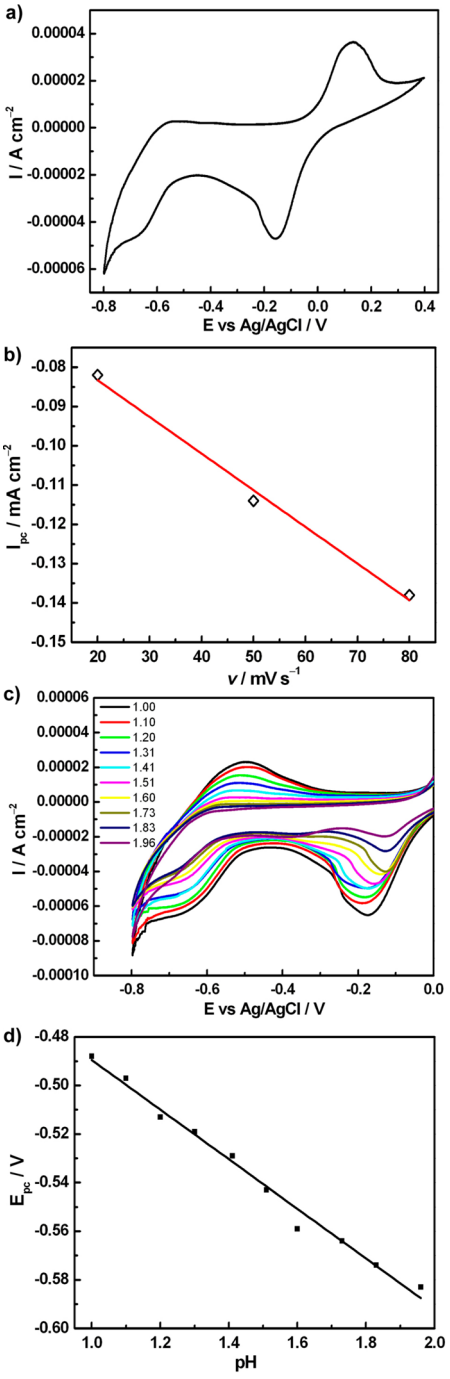

Figure 6. (a) Cyclic voltammogram of **1**-CPE in pH = 1.51, 0.5 mol·L^{-1} Na_2SO_4 + H_2SO_4 aqueous solution. (b) Variation of cathodic peak currents of the W^{VI}-based wave with the scan rate for **1**-CPE. (c) Variation of cyclic voltammograms of **1**-CPE with the pH value. (d) Variation of cathodic peak potentials E_{pc} of the W^{VI}-based wave of **1**-CPE as a function of the pH value. Scan rate: 50 mV s^{-1}.

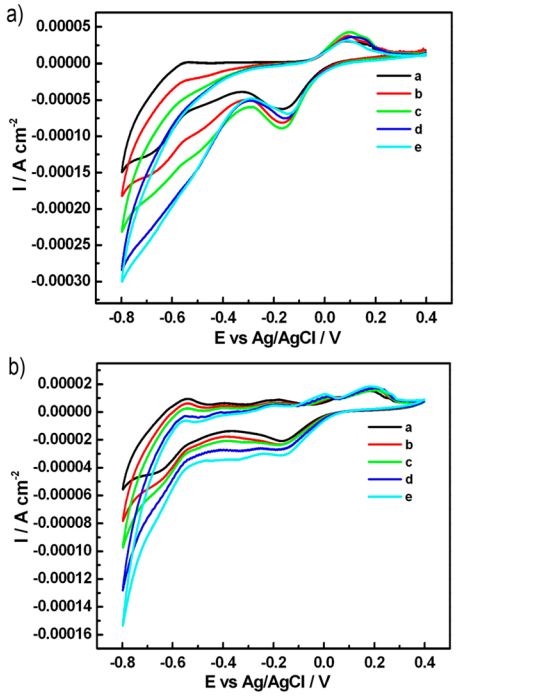

Figure 7. (a) Cyclic voltammograms of **1**-CPE in pH = 1.51, 0.5 mol·L^{-1} Na_2SO_4 + H_2SO_4 aqueous solution containing various concentrations ((a) 3×10^{-3}, (b) 7×10^{-3}, (c) 1.1×10^{-2}, (d) 1.5×10^{-2}, (e) 1.9×10^{-2} mol·L^{-1}) of $NaNO_2$. (b) Cyclic voltammograms of **1**-CPE in pH = 1.51, 0.5 mol·L^{-1} Na_2SO_4 + H_2SO_4 aqueous solution containing various concentrations ((a) 3×10^{-3}, (b) 7×10^{-3}, (c) 1.1×10^{-2}, (d) 1.5×10^{-2}, (e) 1.9×10^{-2} mol·L^{-1}) of $NaBrO_3$. Scan rate: 50 mV s^{-1}.

that, when the pH increases, the current decreases and the entire cyclic voltammogram is shifted in the negative potential direction. Even though the POM is not diffusing freely in solution and reacts mainly in the interfacial region, this feature underscores, once again, the important role of protons in the electrochemistry of POMs.[16c] Figure 6d shows variation of cathodic peak potentials of the W^{VI}-based wave as a function of the pH of the solution. The pH varies in the range of 1.00−1.96, the cathodic peak potentials of the W^{VI}-based wave shift negatively with the increase in the pH, and the plot of the cathodic peak potential (E_{pc}) versus the pH shows good linearity (Figure 6d). The slope of the E_{pc}/pH line is about 102 mV, which indicates the addition of two protons to the reduced forms of **1** when one electron is transferred.

It is well-known that POMs have been extensively exploited in electrocatalytic reductions in the past several years due to their ability to undergo reversible multielectron redox processes.[16b,24] For instance, Keita et al. reported that two-electron-reduced $SiMo_{12}O_{40}^{4-}$ can reduce nitrite in acidic solution.[25] Nohra et al. observed the high electrocatalytic efficiency for the hydrogen evolution reaction of POM-based metal−organic frameworks, $(TBA)_3[PMo^{V}_{8}Mo^{VI}_{4}O_{36}(OH)_4Zn_4][C_6H_3(COO)_3]_{4/3}\cdot 6H_2O$, $(TBA)_3[PMo^{V}_{8}Mo^{VI}_{4}O_{37}(OH)_3Zn_4][C_6H_3(COO)_3]$, and $(TBA)_3[PMo^{V}_{8}Mo^{VI}_{4}O_{37}(OH)_3Zn_4][C_6H_3(COO)_3]\cdot 8H_2O$.[16b] Peng and co-workers investigated the electrocatalytic activity of $(pbpy)_4H[PMo_{12}O_{40}(VO)]$-CPE and $(pbpy)_4H_4[SiMo_{12}O_{40}]$-CPE for the reduction of chlorate.[24a] In the present paper, **1**-CPE and **2**-CPE were employed to probe the electrocatalytic reduction of nitrite and bromate in 0.5 mol·L^{-1} Na_2SO_4 + H_2SO_4 aqueous solution (pH = 1.51). Nitrite is a common pollutant from both agricultural and industrial sources, and its direct electroreduction requires a large overpotential at most electrode surfaces, and no obvious response is observed at a bare CPE.[26] In our experiments, we find that **1**-CPE and **2**-CPE display the electrocatalytic activity toward the reduction of NO_2^- in the acidic sulfate medium in the range of 0.4 to −0.8 V, as shown in Figure 7a and Figure S13a (Supporting Information). It can be clearly seen that, with addition of nitrite, the reduction peak

dx.doi.org/10.1021/cg400746n | *Cryst. Growth Des.* 2013, 13, 4368−4377

currents of the Cu^{II}-based wave is less affected, whereas the reduction peak currents of the W^{VI}-based wave increase gradually and the corresponding oxidation peak currents decrease gradually. The results show that the reduction of nitrite is mainly mediated by the reduced species of tungsten−oxo clusters in **1** and **2**. Actually, such a phenomenon has been previously encountered.[16c,26b] From the viewpoit of medicine, bromate is suspected to act as a human carcinogen,[27] so the monitoring or removal of this species is of interest as it is present in drinking water samples as a byproduct of ozone disinfection and is often used as a food additive.[28] Generally, the reduction of bromate is totally irreversible at a glassy carbon electrode in acidic aqueous solution and does not take place prior to the evolution of hydrogen.[17b] Experiments have attested that the reduction of bromate can readily be catalyzed by the mixed-valence molybdenum or tungsten species.[29] To test the electrocatalytic ability of **1**-CPE and **2**-CPE toward the reduction of BrO_3^-, CV measurements of **1**-CPE and **2**-CPE in 0.5 mol·L^{-1} Na_2SO_4 + H_2SO_4 aqueous solution containing various concentrations of $NaBrO_3$ have been carried out at room temperature. It can be seen from Figure 7b and Figure S13b (Supporting Information) that the onset of the catalytic process is triggered by the W^{VI}-based wave. With the addition of BrO_3^-, the cathodic current of the W^{VI}-based wave rises; meanwhile, the corresponding anodic current gradually decreases while the Cu^{II}-based wave is almost unaffected by the addition of BrO_3^-. The phenomenon suggests that bromate is reduced by the reduced species of tungsten components.[17b,27] In addition, to check the stability of catalyst **1** after the electrocatalytic reduction of nitrite and bromate, the IR spectra of **1** and **1**-CPE before electrocatalysis and **1**-CPE after electrocatalysis are compared (Figure S14, Supporting Information). Because the reduction of nitrite or bromate is mainly mediated by the reduced species of tungsten-oxo clusters in **1**, the comparison of the IR spectra is concentrated on the characteristic vibration bands of the POM cluster in the low-wavenumber region. The result exhibits that four characteristic vibration bands, $\nu(W-O_t)$, $\nu(Ge-O_a)$, $\nu(W-O_b)$, and $\nu(W-O_c)$, of **1**-CPE before electrocatalysis and **1**-CPE after electrocatalysis are not shifted and no new vibration band is observed in IR spectra in comparison with those of the original sample **1**, which suggests that the catalyst **1** is stable after electrocatalysis. The similar case is observed for **2** (Figure S15, Supporting Information). By and large, the results indicate that the **1**-CPE and **2**-CPE have obvious electrocatalytic activities for the nitrite and bromate reduction.

CONCLUSIONS

In summary, we have successfully prepared two unusual 1D copper-bridged tetrahedral POM nanoclusters with a tetrameric RE core and GT vertexes $Na_3H_7[Cu(en)_2]_5[Cu(en)_2(H_2O)]_2[RE_4Ge_4W_{46}O_{164}(H_2O)_3]\cdot nH_2O$ (RE = Gd^{III}, n = 25 for **1**; RE = Y^{III}, n = 23 for **2**), which have been structurally characterized. In particular, the most remarkable feature of **1** and **2** is the occurrence of an unprecedented tetrahedral RE-substituted GT nanoscale subunit, $\{[(\alpha\text{-}GeW_{11}O_{39}RE)_2(\mu_3\text{-}WO_4)(\alpha\text{-}GeW_{11}O_{39}RE(H_2O))](\mu_4\text{-}WO_4)[\alpha\text{-}GeW_{11}O_{39}RE(H_2O)_2]\}^{24-}$, in which four Keggin-type $[\alpha\text{-}GeW_{11}O_{39}RE(H_2O)_n]^{5-}$ (n = 0, 1, 2) spheres are fused together with the help of two WO_4^{2-} ions. It should be noted that the construction mode of such tetrahedral nanoclusters is first discovered. Furthermore, the solid-state electrochemical and electrocatalytic properties of **1** and **2** have been evaluated. Both **1**-CPE and **2**-CPE have obvious electrocatalytic activities for nitrite and bromate reduction. This work opens up a door for exploring the extended structures created by large TM−RE containing POM fragments. More giant TM−RE containing POMs with extended structures can be expected through this approach in the future. More importantly, chiral organic ligands will be introduced to this system to control the charge distribution of microstructures of desired materials, further leading to the noncoincidence of the centers for the positive charges and negative charges, and thus, TM−RE containing POM-based functional materials with ferroelectricity and piezoelectricity will be prepared.

ASSOCIATED CONTENT

Supporting Information

The details during the course of the refinements of structures of **1** and **2**; summary of phases obtained from lacunary Keggin GT precursors; IR spectra of **1** and **2**; related structural figures; TGA figures of **1** and **2**; BVS values of the oxygen atoms in **1**; hydrogen-bonding interactions in **1**; adsorption isotherms of **1** and **2**; cyclic voltammograms of **2**; and crystal data in CIF format. This material is available free of charge via the Internet at http://pubs.acs.org. Crystallographic data have been deposited at the Cambridge Crystallographic Data Center, CCDC 921538 for **1** and for 921539. These data can be obtained free of charge from the Cambridge Crystallographic Data Centre via www.ccdc.cam.ac.uk/data_ request/cif.

AUTHOR INFORMATION

Corresponding Authors

*E-mail: zhaojunwei@henu.edu.cn (J. W. Zhao). Fax: (+86) 378 3886876.
*E-mail: zhj@fjirsm.ac.cn (J. Zhang).
*E-mail: jyniu@henu.edu.cn (J. Y. Niu).

Notes

The authors declare no competing financial interest.

ACKNOWLEDGMENTS

This work was supported by the 973 program (2011CB932504 and 2012CB821705), the Natural Science Foundation of China (21073191, 21101055, 21221001, 21071042, 21071043), the China Postdoctoral Science Foundation Funded Project (201104392, 20100470996), the Natural Science Foundation of Henan Province (122300410106, 102300410093), the Foundation of State Key Laboratory of Structural Chemistry (20120013), the 2012 Young Backbone Teachers Foundation from Henan Province, the Postdoctoral Science Foundation of Henan University (BH2010003), the Foundation of Education Department of Henan Province (2009A150003, 2010B150006), and the Students Innovative Pilot Plan of Henan University (2012, 2013).

REFERENCES

(1) (a) Borras-Almenar, J. J.; Coronado, E.; Müller, A.; Pope, M. T. *Polyoxometalate Molecular Science*; Kluwer Academic Publishers: Dordrecht, The Netherlands, 2003. (b) Rhule, J. T.; Hill, C. L.; Judd, D. A. *Chem. Rev.* **1998**, *98*, 327−357. (c) Mizuno, N.; Yamaguchi, K.; Kamata, K. *Coord. Chem. Rev.* **2005**, *249*, 1944−1956. (d) Absillis, G.; Parac-Vogt, T. N. *Inorg. Chem.* **2012**, *51*, 9902−9910. (e) Long, D. L.; Burkholder, E.; Cronin, L. *Chem. Soc. Rev.* **2007**, *36*, 105−121.

(2) Fang, X.; Kögerler, P.; Furukawa, Y.; Speldrich, M.; Luban, M. *Angew. Chem., Int. Ed.* **2011**, *50*, 5212−5216.

(3) Duval, S.; Pilette, M.; Marrot, J.; Simonnet-Jégat, C.; Sokolov, M.; Cadot, E. *Chem.—Eur. J.* **2008**, *14*, 3457−3466.
(4) (a) Fukaya, K.; Yamase, T. *Angew. Chem., Int. Ed.* **2003**, *42*, 654−658. (b) Godin, B.; Chen, Y. G.; Vaissermann, J.; Ruhlmann, L.; Verdaguer, M.; Gouzerh, P. *Angew. Chem., Int. Ed.* **2005**, *44*, 3072−3075. (c) Bassil, B. S.; Dickman, M. H.; Römer, I.; von der Kammer, B.; Kortz, U. *Angew. Chem., Int. Ed.* **2007**, *46*, 6192−6195. (d) Zhao, J. W.; Jia, H. P.; Zhang, J.; Zheng, S. T.; Yang, G. Y. *Chem.—Eur. J.* **2007**, *13*, 10030−10045. (e) Zhang, Z.; Qi, Y.; Qin, C.; Li, Y.; Wang, E.; Wang, X.; Su, Z.; Xu, L. *Inorg. Chem.* **2007**, *46*, 8162−8169. (f) Hussain, F.; Conrad, F.; Patzke, G. R. *Angew. Chem., Int. Ed.* **2009**, *48*, 9088−9091. (g) Reinoso, S.; Giménez-Marqués, M.; Galán-Mascarós, J.; Vitoria, P.; Gutiérrez-Zorrilla, J. M. *Angew. Chem., Int. Ed.* **2010**, *49*, 8384−8388. (h) Bassil, B. S.; Ibrahim, M.; Al-Oweini, R.; Asano, M.; Wang, Z.; van Tol, J.; Dalal, N. S.; Choi, K. Y.; Biboum, R. N.; Keita, B.; Nadjo, L.; Kortz, U. *Angew. Chem., Int. Ed.* **2011**, *50*, 5961−5964.
(5) (a) Zheng, S. T.; Zhang, J.; Clemente-Juan, J. M.; Yuan, D. Q.; Yang, G. Y. *Angew. Chem., Int. Ed.* **2009**, *48*, 7176−7179. (b) Zhao, J. W.; Shi, D. Y.; Chen, L. J.; Ma, P. T.; Wang, J. P.; Niu, J. Y. *CrystEngComm* **2011**, *13*, 3462−3469. (c) Mitchell, S. G.; Streb, C.; Miras, H. N.; Boyd, T.; Long, D. L.; Cronin, L. *Nat. Chem.* **2010**, *2*, 308−312.
(6) (a) Wu, C. D.; Lu, C. Z.; Zhuang, H. H.; Huang, J. S. *J. Am. Chem. Soc.* **2002**, *124*, 3836−3837. (b) Mialane, P.; Dolbecq, A.; Rivière, E.; Marrot, J.; Sécheresse, F. *Eur. J. Inorg. Chem.* **2004**, 33−36. (c) Chen, W. L.; Li, Y. G.; Wang, Y. H.; Wang, E. B.; Zhang, Z. M. *Dalton Trans.* **2008**, 865−867.
(7) Bi, L.-H.; Kortz, U.; Nellutla, S.; Stowe, A. C.; van Tol, J.; Dalal, N. S.; Keita, B.; Nadjo, L. *Inorg. Chem.* **2005**, *44*, 896−903.
(8) (a) Sheldrick, G. M. *SADABS: Program for Empirical Absorption Correction of Area Detector Data*; University of Göttingen: Göttingen, Germany, 1996. (b) Sheldrick, G. M. *SHELXS97: Program for Crystal Structure Solution*; University of Göttingen: Göttingen, Germany, 1997. (c) Sheldrick, G. M. *SHELXL97: Program for Crystal Structure Refinement*; University of Göttingen: Göttingen, Germany, 1997.
(9) (a) Howell, R. C.; Perez, F. G.; Jain, S.; Horrocks, W. D., Jr.; Rheingold, A. L.; Francesconi, L. C. *Angew. Chem., Int. Ed.* **2001**, *40*, 4031−4034. (b) Kortz, U.; Hussain, F.; Reicke, M. *Angew. Chem., Int. Ed.* **2005**, *44*, 3773−3777. (c) Zhang, Z.-M.; Yao, S.; Li, Y.-G.; Wang, Y.-H.; Qi, Y.-F.; Wang, E.-B. *Chem. Commun.* **2008**, 1650−1652. (d) Zhao, J.-W.; Wang, C.-M.; Zhang, J.; Zheng, S.-T.; Yang, G.-Y. *Chem.—Eur. J.* **2008**, *14*, 9223−9239. (e) Fang, X.; Anderson, T. M.; Hill, C. L. *Angew. Chem., Int. Ed.* **2005**, *44*, 3540−3544. (f) Zhao, J.-W.; Zhang, J.; Zheng, S.-T.; Yang, G.-Y. *Chem. Commun.* **2008**, 570−572. (g) Wu, Q.; Li, Y.-G.; Wang, Y.-H.; Wang, E.-B.; Zhang, Z.-M.; Clérac, R. *Inorg. Chem.* **2009**, *48*, 1606−1612. (h) Bi, L.-H.; Wang, E.-B.; Peng, J.; Huang, R.-D.; Xu, L.; Hu, C.-W. *Inorg. Chem.* **2000**, *39*, 671−679. (i) Chen, W.; Li, Y.; Wang, Y.; Wang, E.; Su, Z. *Dalton Trans.* **2007**, 4293−4301. (j) Kim, G.-S.; Zeng, H.; Vanderveer, D.; Hill, C. L. *Angew. Chem., Int. Ed.* **1999**, *38*, 3205−3207. (k) Mialane, P.; Dolbecq, A.; Marrot, J.; Rivière, E.; Sécheresse, F. *Angew. Chem., Int. Ed.* **2003**, *42*, 3523−3526. (l) Nsouli, N. H.; Ismail, A. H.; Helgadottir, I. S.; Dickman, M. H.; Clemente-Juan, J. M.; Kortz, U. *Inorg. Chem.* **2009**, *48*, 5884−5890. (m) Li, B.; Zhao, J.-W.; Zheng, S.-T.; Yang, G.-Y. *Inorg. Chem.* **2009**, *48*, 8294−8303.
(10) (a) Bi, L.-H.; Kortz, U.; Keita, B.; Nadjo, L. *Dalton Trans.* **2004**, 3184−3190. (b) Bi, L.-H.; Kortz, U.; Dickmann, M. H.; Keita, B.; Nadjo, L. *Inorg. Chem.* **2005**, *44*, 7485−7493. (c) Wang, J.-P.; Zhao, J.-W.; Duan, X.-Y.; Niu, J.-Y. *Cryst. Growth Des.* **2006**, *6*, 507−513. (d) Wang, J.-P.; Duan, X.-Y.; Du, X.-D.; Niu, J.-Y. *Cryst. Growth Des.* **2006**, *6*, 2266−2270. (e) Bi, L.-H.; Chubarova, E. V.; Nsouli, N. H.; Dickman, M. H.; Kortz, U.; Keita, B.; Nadjo, L. *Inorg. Chem.* **2006**, *45*, 8575−8583. (f) Tan, R.; Wang, X.; Chai, F.; Lan, Y.; Su, Z. *Inorg. Chem. Commun.* **2006**, *9*, 1331−1334. (g) Sun, C.-Y.; Liu, S.-X.; Wang, C.-L.; Xie, L.-H.; Zhang, C.-D.; Gao, B.; Su, Z.-M.; Jia, H.-Q. *J. Mol. Struct.* **2006**, *785*, 170−175. (h) Zhao, J.-W.; Li, B.; Zheng, S.-T.; Yang, G.-Y. *Cryst. Growth Des.* **2007**, *7*, 2658−2664. (i) Nsouli, N. H.; Mal, S. S.; Dickman, M. H.; Kortz, U.; Keita, B.; Nadjo, L.; Clemente-Juan, J. M. *Inorg. Chem.* **2007**, *46*, 8763−8770. (j) Zhang, Z.; Wang, E.; Li, Y.; Qi, Y.; Tan, H. *J. Mol. Struct.* **2007**, *843*, 128−131. (k) Reinoso, S.; Dickman, M. H.; Praetorius, A.; Piedra-Garza, L. F.; Kortz, U. *Inorg. Chem.* **2008**, *47*, 8798−8806. (l) Gan, X.; Zhang, Z.; Yao, S.; Chen, W.; Wang, E.; Zhang, H. *J. Cluster Sci.* **2008**, *19*, 401−410. (m) Zhao, J.-W.; Zhang, J.; Song, Y.; Zheng, S.-T.; Yang, G.-Y. *Eur. J. Inorg. Chem.* **2008**, 3809−3819. (n) Zhao, J.-W.; Zheng, S.-T.; Yang, G.-Y. *J. Solid State Chem.* **2008**, *181*, 2205−2216. (o) Mitchell, S. G.; Khanra, S.; Miras, H. N.; Boyd, T.; Long, D.-L.; Cronin, L. *Chem. Commun.* **2009**, 2712−2714. (p) Li, Y. G.; Xu, L.; Gao, G. G.; Jiang, N.; Liu, H.; Li, F. Y.; Yang, Y. Y. *CrystEngComm* **2009**, *11*, 1512−1514. (q) Zhao, J.-W.; Zheng, S.-T.; Li, Z.-H.; Yang, G.-Y. *Dalton Trans.* **2009**, 1300−1306. (r) Copping, R.; Talbot-Eeckelaers, C.; Collison, D.; Helliwell, M.; Gaunt, A. J.; May, I.; Reilly, S. D.; Scott, B. L.; McDonald, R. D.; Valenzula, O. A.; Jones, C. J.; Sarsfield, M. J. *Dalton Trans.* **2009**, 5609−5611. (s) Li, B.; Zhao, J.-W.; Zheng, S.-T.; Yang, G.-Y. *Inorg. Chem. Commun.* **2009**, *12*, 69−71. (t) Chen, L.; Li, L.; Liu, B.; Xue, G.; Hua, H.; Fu, F.; Wang, J. *Inorg. Chem. Commun.* **2009**, *12*, 1035−1037. (u) Chen, L.; Liu, Y.; Chen, S.; Hu, H.; Fu, F.; Wang, J.; Xue, G. *J. Cluster Sci.* **2009**, *20*, 331−340. (v) Mal, S. S.; Nsouli, N. H.; Carraro, M.; Sartorel, A.; Scorrano, G.; Oelrich, H.; Walder, L.; Bonchio, M.; Kortz, U. *Inorg. Chem.* **2010**, *49*, 7−9. (w) Reinoso, S.; Galán-Mascarós, J. R. *Inorg. Chem.* **2010**, *49*, 377−379. (x) Khoshnavazi, R.; Gholamyan, S. *J. Coord. Chem.* **2010**, *63*, 3365−3372. (y) Reinoso, S.; Galán-Mascarós, J. R.; Lezama, L. *Inorg. Chem.* **2011**, *50*, 9587−9593.
(11) (a) Chen, L. J.; Shi, D. Y.; Zhao, J. W.; Wang, Y. L.; Ma, P. T.; Wang, J. P.; Niu, J. Y. *Cryst. Growth Des.* **2011**, *11*, 1913−1923. (b) Niu, W. J.; Shi, D. Y.; Zhao, J. W.; Cai, X. M.; Chen, L. J. *Inorg. Chem. Commun.* **2012**, *17*, 79−83. (c) Zhao, J. W.; Shi, D. Y.; Chen, L. J.; Li, Y. Z.; Ma, P. T.; Wang, J. P.; Niu, J. Y. *Dalton Trans.* **2012**, *41*, 10740−10751. (d) Chen, L. J.; Shi, D. Y.; Zhao, J. W.; Wang, Y. L.; Ma, P. T.; Niu, J. Y. *Inorg. Chem. Commun.* **2011**, *14*, 1052−1056.
(12) Kortz, U.; Matta, S. *Inorg. Chem.* **2001**, *40*, 815−817.
(13) Ibrahim, M.; Lan, Y.; Bassil, B. S.; Xiang, Y.; Suchopar, A.; Powell, A. K.; Kortz, U. *Angew. Chem., Int. Ed.* **2011**, *50*, 4708−4711.
(14) Brown, I. D.; Altermatt, D. *Acta Crystallogr.* **1985**, *B41*, 244−247.
(15) Mialane, P.; Dolbecq, A.; Marrot, J.; Rivière, E.; Sécheresse, F. *Angew. Chem., Int. Ed.* **2003**, *42*, 3523−3526.
(16) (a) Hill, C. L. *Chem. Rev.* **1998**, *98*, 1−389. (b) Nohra, B.; Moll, H. E.; Albelo, L. M. R.; Mialane, P.; Marrot, J.; Mellot-Draznieks, C.; O'Keeffe, M.; Biboum, R. N.; Lemaire, J.; Keita, B.; Nadjo, L.; Dolbecq, A. *J. Am. Chem. Soc.* **2011**, *133*, 13363−13374. (c) Keita, B.; de Oliveira, P.; Nadjo, L.; Kortz, U. *Chem.—Eur. J.* **2007**, *13*, 5480−5491.
(17) (a) Sadakane, M.; Stechhan, E. *Chem. Rev.* **1998**, *98*, 219−238. (b) Wang, X.; Wang, E.; Lan, Y.; Hu, C. *Electroanalysis* **2002**, *14*, 1116−1121.
(18) (a) Salimi, A.; Korani, A.; Hallaj, R.; Khoshnavazi, R.; Hadadzadeh, H. *Anal. Chim. Acta* **2009**, *635*, 63−70. (b) Nellutla, S.; van Tol, J.; Dalal, N. S.; Bi, L. H.; Kortz, U.; Keita, B.; Nadjo, L.; Khitrov, G. A.; Marshall, A. G. *Inorg. Chem.* **2005**, *44*, 9795−9806.
(19) (a) Bassil, B. S.; Kortz, U.; Tigan, A. S.; Clemente-Juan, J. M.; Keita, B.; Oliveira, P.; Nadjo, L. *Inorg. Chem.* **2005**, *44*, 9360−9368. (b) Mbomekalle, I. M.; Keita, B.; Nierlich, M.; Kortz, U.; Berthet, P.; Nadjo, L. *Inorg. Chem.* **2003**, *42*, 5143−5152.
(20) Ammam, M.; Easton, E. B. *Electrochim. Acta* **2011**, *56*, 2847−2855.
(21) Keita, B.; Essaadi, K.; Nadjo, L. *J. Electroanal. Chem. Interfacial Electrochem.* **1989**, *259*, 127−146.
(22) (a) Brett, C. M. A.; Brett, A. M. O. *Electrochemistry Principles, Methods, and Applications*; Oxford University Press: Oxford, U.K., 1993. (b) Wang, J. *Analytical Electrochemistry*; VCH: New York, 1994.
(23) Qu, J.; Zou, X.; Liu, B.; Dong, S. *Anal. Chim. Acta* **2007**, *599*, 51−57.
(24) (a) Han, Z.; Zhao, Y.; Peng, J.; Feng, Y.; Yin, J.; Liu, Q. *Electroanalysis* **2005**, *17*, 1097−1102. (b) Toth, J. E.; Anson, F. C. *J. Am. Chem. Soc.* **1989**, *111*, 2444−2451.

(25) Keita, B.; Belhouari, A.; Nadjo, L.; Contant, R. *J. Electroanal. Chem.* **1995**, *381*, 243−250.
(26) (a) Keita, B.; Nadjo, L. *J. Electroanal. Chem. Interfacial Electrochem.* **1987**, *227*, 77−98. (b) Wang, X.; Hu, H.; Tian, A.; Lin, H.; Li, J. *Inorg. Chem.* **2010**, *49*, 10299−10306.
(27) (a) Moore, M. M.; Chen, T. *Toxicology* **2006**, *221*, 190−196. (b) Bonacquisti, T. P. *Toxicology* **2006**, *221*, 145−148.
(28) Rodriguez-Albelo, L. M.; Ruiz-Salvador, A. R.; Sampieri, A.; Lewis, D. W.; Gómez, A.; Nohra, B.; Mialane, P.; Marrot, J.; Sécheresse, F.; Mellot-Draznieks, C.; Biboum, R. N.; Keita, B.; Nadjo, L.; Dolbecq, A. *J. Am. Chem. Soc.* **2009**, *131*, 16078−16087.
(29) (a) Wang, B.; Dong, S. *J. Electroanal. Chem.* **1994**, *379*, 207−214. (b) Lahr, S. K.; Finklea, H. O.; Schultz, F. A. *J. Electroanal. Chem. Interfacial Electrochem.* **1984**, *163*, 237−255.